European Journal of Pharmacology 890 (2021) 173670

Contents lists available at ScienceDirect

European Journal of Pharmacology

journal homepage: www.elsevier.com/locate/ejphar

Full length article

Therapeutic effect of uridine phosphorylase 1 (UPP1) inhibitor on liver fibrosis *in vitro* and *in vivo*

Elisa Feller Gonçalves da Silva [a,*], Bruna Pasqualotto Costa [a], Marcella Tornquist Nassr [a], Bruno de Souza Basso [a], Matheus Scherer Bastos [a], Géssica Luana Antunes [a], Camille Kirinus Reghelin [a], Maria Claudia Rosa Garcia [a], Vitor Giancarlo Schneider Levorse [a], Leonardo Pfeiff Carlessi [a], Krist Helen Antunes Fernandes [b], Carine Raquel Richter Schmitz [c], Gabriela Viegas Haute [a], Carolina Luft [a], Eliane Santarém [d], Florencia María Barbé-Tuana [e], Márcio Vinícius Fagundes Donadio [a], Luiz Augusto Basso [f], Pablo Machado [f], Jarbas Rodrigues de Oliveira [a]

[a] *Laboratório de Pesquisa Em Biofísica Celular e Inflamação, Pontifícia Universidade Católica Do Rio Grande Do Sul (PUCRS), Porto Alegre, Rio Grande do Sul, 90619-900, Brazil*
[b] *Laboratório de Imunologia Clínica e Experimental, Pontifícia Universidade Católica Do Rio Grande Do Sul (PUCRS), Porto Alegre, Rio Grande do Sul, 90619-900, Brazil*
[c] *Programa de Pós-Graduação Em Biologia Celular: Bioquímica, Universidade Federal Do Rio Grande Do Sul (UFRGS), Porto Alegre, Rio Grande do Sul, 90619-900, Brazil*
[d] *Laboratório de Biotecnologia Vegetal, Pontifícia Universidade Católica Do Rio Grande Do Sul (PUCRS), Porto Alegre, Rio Grande do Sul, 90619-900, Brazil*
[e] *Laboratório de Imunobiologia, Pontifícia Universidade Católica Do Rio Grande Do Sul (PUCRS), Porto Alegre, Rio Grande do Sul, 90619-900, Brazil*
[f] *Centro de Pesquisas Em Biologia Molecular e Funcional (CPBMF), Pontifícia Universidade Católica Do Rio Grande Do Sul (PUCRS), TecnoPuc, Porto Alegre, Rio Grande do Sul, 90619-900, Brazil*

ARTICLE INFO

Keywords:
Uridine phosphorylase 1
Hepatic stellate cells
Liver fibrosis
Antifibrotic

ABSTRACT

Potassium 5-cyano-4-methyl-6-oxo-1,6-dihydropyridine-2-olate (CPBMF65) is a potent inhibitor of the uridine phosphorylase 1 (UPP1) enzyme. Its non-ionized analog has already demonstrated biological properties by reducing adverse effects caused by the chemotherapeutic 5-fluorouracil (5-FU). In addition, it has been demonstrated that uridine inhibits inflammation and fibrosis in bleomycin lung injury, decreasing collagen production. The purpose of this study was to investigate the *in vitro* and *in vivo* effects of CPBMF65 on activated hepatic stellate cells (HSC) and on carbon tetrachloride-induced liver fibrosis in mice. After incubation with CPBMF65, decreased cell proliferation and phenotype reversion were observed *in vitro*. In addition, CPBMF65 promoted a protective effect on tetrachloride-induced liver fibrosis in mice, demonstrated by its antifibrotic and anti-inflammatory actions. The results of the present study indicate that the UPP1 inhibitor (CPBMF65) may have potential as a novel therapeutic agent for the treatment of liver fibrosis.

1. Introduction

Liver fibrosis is the pathologic result of inflammatory liver diseases, characterized by activated hepatic stellate cells (HSC) proliferation, inability to store vitamin A in cytoplasmic lipid droplets, and increased expression of α-smooth muscle actin (α-SMA) and profibrotic genes (Basso et al., 2019). It may be associated with chronic injuries, including viral infection, alcohol abuse and steatosis, leading to accumulation of fibrotic matrix rich in collagen and, at later stages, to liver failure and mortality (Bárcena et al., 2019). However, as previously described, liver fibrosis is potentially reversible (Shin et al., 2018).

Antifibrotic agents targeting HSC activation have been proposed as a therapeutic target to liver fibrosis. Uridine phosphorylase is a key enzyme in the pyrimidine salvage pathway, catalyzing the reversible phosphorolysis of uridine (Urd) to uracil and ribose-1-phosphate. The human uridine phosphorylase type 1 (UPP1) is a molecular target of

* Corresponding author.
E-mail address: elisa.feller@acad.pucrs.br (E.F. Gonçalves da Silva).

https://doi.org/10.1016/j.ejphar.2020.173670
Received 18 October 2019; Received in revised form 19 October 2020; Accepted 21 October 2020
Available online 22 October 2020

inhibitors proposed to increase Urd levels to prevent adverse effects of chemotherapeutic agents like 5- fluorouracil (Renck et al., 2010). The therapeutic potential of Urd has also been assessed in disorders such as cystic fibrosis and liver dysfunction (Weinberg et al., 2011). Moreover, the study of Cicko et al. (2015) demonstrated that Urd presents anti-inflammatory and anti-fibrotic effects in animal models of pulmonary fibrosis. In addition, Urd treatment also inhibited the synthesis of collagen, leading to a reduction in collagen deposition in the lung (Cicko et al., 2015).

Selective inhibitors of UPP1 have been proposed to increase Urd levels. Urd is one of the five standard molecules that comprise nucleic acids, involved in cellular processes such as RNA synthesis. Exogenous administration of Urd is not well tolerated, since higher doses would have to be administered in order to obtain significant effects, due to the rapid degradation caused by UPP1 (Pizzorno et al., 2002). The potassium 5-cyano-4-methyl-6-oxo- 1,6-dihydropyridine-2-olate (CPBMF65) is a new molecule synthetized and produced at the Pontifícia Universidade Católica do Rio Grande do Sul (PUCRS). It is an inhibitor of UPP1 and has been tested to verify the 5-fluorouracil toxicity decrease in SW-620 cells (Renck et al., 2013). The present study aimed to investigate the effects of the UPP1 inhibitor, CPBMF65, on hepatic stellate cells (GRX), and on carbon tetrachloride-induced liver fibrosis in mice. We sought to demonstrate the possible potential therapeutic effect of CPBMF65 on liver fibrosis.

2. Materials and methods

2.1. HSC cell culture

GRX hepatic stellate cell line is an immortalized lineage of liver cells obtained from hepatic 18 granulomas of mice infected with *Schistosoma mansoni*. This lineage of HSCs normally presents a myofibroblast transitional phenotype, between the quiescent (normal) and activated stages (myofibroblast phenotype). GRX cell line was obtained from Rio de Janeiro Cell Bank (Federal University, Brazil). The medium used for cell culture was Dulbecco's Modified Eagle Medium (DMEM), supplemented with 5% fetal bovine serum (FBS) (Invitrogen, USA), 2 g/l HEPES buffer, 3.7 g/l $NaHCO_3$, 1% penicillin and streptomycin (Invitrogen, USA), and pH 7.4. Experiments were performed with cells between the fifth and twelfth passages in 24-well tissue culture plates with density of 3×10^3 cells per well ($1{,}57 \times 10^3$ cells/cm^2). Cells were incubated with CPBMF65 for 120 h at 37 °C under a humidified atmosphere containing 5% CO_2. All experiments were performed three times.

2.2. In vitro treatment with CPBMF65

Plates were incubated at 37 °C in a humidified atmosphere with 5% CO_2 for 120 h, aiming to perform a dose-response curve and also to determine the cytotoxicity of CPBMF65. Different concentrations (7.5, 15, 45 and 90 μM) diluted in DMEM medium with 5% FBS were tested. N-acetylcysteine (NAC; 400 μM, Farmashop, Brazil), was used as a positive control. The control group consisted of GRX cells on culture medium for all experiments. The 120-h treatment time was determined after a previous time-curve was performed in our laboratory. As previous works of our group (Basso et al., 2019; De Mesquita et al., 2013) reported that the process of GRX cell phenotype reversal (lipogenesis) may take between 3 and 7 days to be observed in Oil red staining, depending on the type of treatment. In the present work the process was evidenced mainly after 5 days of treatment with CPBMF65 and for this reason we chose this time to perform incubations. All experiments were performed three times.

2.3. Evaluation of cellular proliferation

The Trypan Blue exclusion assay was used to assess viability and cell growth/proliferation. Cells were seeded and treated as described above. After 120 h of incubation, the number of viable cells was determined by mixing 25 μμl of cell suspension and 25 μl of 0.4% Trypan Blue (Sigma-Aldrich, USA) using a Neubauer hemocytometer and optical microscope (Nikon Optiphot, Japan). Blue cells were counted as dead cells and those that did not absorb the dye, as living cells. The results were expressed as the absolute number of cells per culture well.

2.4. Measurement of lactate dehydrogenase

The cytotoxicity of the treatments was evaluated by the presence of the lactate dehydrogenase (LDH) enzyme in the external environment, since its release (lactate dehydrogenase enzyme located in the cytoplasm) in the culture medium is considered evidence of cell membrane rupture. Enzyme activity was measured in both (supernatants and lysates) using the colorimetric lactate dehydrogenase kit (Labtest, Brazil). As a control of cell lysis, we have used Tween 5% (Sigma-Aldrich, Germany) in the culture medium. LDH release was calculated by measuring the absorbance at 340 nm using an ELISA microplate reader. All experiments were performed in triplicate and repeated three times.

2.5. Nuclear morphometric analysis (NMA)

The NMA is based on the evaluation of the size and shape of the nucleus of eukaryotic cells *in vitro*. This technique enables the assessment of the number of cells which present nuclear morphology phenotypically compatible with senescent or apoptotic cells. Cells were seeded in 24-well plates with a cell density of 5×10^4 per well and treated with the selected doses of CPBMF65 (7.5 and 90 μM). After 120 h of treatment, the culture medium was discarded and four steps were performed: (1) labeling of the nuclei with DAPI (4′, 6- diamidino-2-phenylindole), a fluorescent dye that binds strongly to the adenine-rich regions and thymine in DNA sequences (Kim et al., 2012); (2) acquisition of images by an inverted fluorescence microscope (Eclipse TE2000-S, Nikon, Japan); (3) obtaining the morphometric data (Image Pro-Plus 4.5 software, Media Cybernetics, USA); (4) data analysis (Excel, 2013), according to the protocol previously described (Sperotto, 2014). As an apoptosis positive control, 2.5 μM Cisplatin (CDDP) was used, and as a senescence positive control, 150 μM hydrogen peroxide (H_2O_2) was used (Zdanov, 2006).

2.6. Evaluation of cell death by apoptosis

Cell death by apoptosis was performed using Annexin V-FITC flow cytometry kit (QuatroG, Brazil). After 120 h of treatment with selected concentrations of CPBMF65 (7.5 and 90 μM), H_2O_2 (150 μM) and CDDP (2.5 μM), the culture medium was discarded, cells were harvested and washed with PBS. Then, cells were re-suspended in 100 μl of binding buffer at a cell density of 1×10^6 cells/ml and incubated with 4 μl of Annexin V- FITC and 4 μl of Propidium Iodide (PI) for 15 min at room temperature protected from light. Fluorescence analysis was performed by FACSCanto II Flow Cytometer (BD, Becton- Dickinson, USA) and data were analyzed using FlowJo 7.6.5 software (Tree Star Inc., Ashland, OR).

2.7. Evaluation of senescence

Senescence-associated β-galactosidase (SA-β-gal) activity can be detected thought 5- dodecanoylaminofluorescein di-β-D-galactopyranoside (C_{12}FDG), a fluorogenic substrate for β-galactosidase (Debacq-Chainiaux et al., 2009). After 120 h of treatment with CPBMF65 (7.5 and 90 μM), H_2O_2 (150 μM) and CDDP (2.5 μM) cells were harvested, treated with a final concentration of 100 nM of Bafilomycin A1 to neutralize the acidic pH of lysosomes, and incubated at 37 °C, 5% CO_2. After 1 h, cells were stained with C_{12}FDG (Invitrogen, Thermo Fisher, Inc., USA) diluted in fresh culture media at a final concentration of 33 μM and incubate 1 h at 37 °C, 5% CO_2. Cells were

washed in PBS and fluorescence was performed by FACSCanto II Flow Cytometer (BD, Becton-Dickinson, USA) and data were analyzed using FlowJo 7.6.5 software (Tree Star Inc., Ashland, OR).

Histone γ-H2AX, a sensitive marker of double-stranded DNA breaks, is increased in damaged and senescent cells (Sharma et al., 2012). After 120 h of treatment with CPBMF65 (7.5 and 90 μM), H_2O_2 (150 μM) and CDDP (2.5 μM) cells were harvested, fixed with CytoFix Fixation Buffer (BD, Becton-Dickinson, USA), and permeabilized with Perm/Wash 1*X* (BD, Becton-Dickinson, USA) and Perm Buffer III (BD, Becton-Dickinson, USA). After, cells were collected by centrifugation and resuspended in a buffer solution (2% FBS diluted in PBS) with PE mouse anti-H2AX (pS139) (BD, Becton-Dickinson, USA #562377) for 40 min. Cells were washed in buffer and the fluorescence was performed by FACSCanto II Flow Cytometer (BD, Becton-Dickinson, USA) and data were analyzed using FlowJo 7.6.5 software (Tree Star Inc., Ashland, OR).

2.8. Detection of GRX cells lipid droplets

The estimation of lipid droplets accumulation in the cells was observed using the Oil Red (ORO; Sigma Chemical Co., USA) assay. After 120 h of treatment with selected concentrations of CPMF65 (7.5 and 90 μM) and NAC 400 μM, cells were fixed with 10% formaldehyde for 1 h and stained with ORO. Intracellular lipid accumulation was observed after 30 min, using an inverted light microscope at a magnification of 400*x*. The ORO was extracted using isopropanol and the absorbance was read at 340 nm using an ELISA microplate reader. Specific lipid content was calculated as the ratio of absorbance value obtained for ORO and the number of counted cells.

2.9. Assessment of GRX cell contraction by collagen gel analyses

Collagen from rat tail tendons was extracted and prepared as previously described (Rajan et al., 2006). Collagen gels (125 μl of four time's concentrated DMEM medium and 125 μl of 4 mg/ml rat tail tendon collagen) were impregnated with 1×10^5 cells resuspended in 250 μl of PBS. Gels were added to a 24-well plate, left to polymerize for 30 min at 37 °C, detached and suspended in 600 μl of DMEM with 5% FBS alone or with CPBMF65 and NAC. Images were obtained after 24 h and the surface of the area of each gel was determined as the percentage of well area, using the software Image-Pro Plus 4.5 (Media Cybernetics, USA).

2.10. Animals

Male BALB/c mice (8–12 weeks old) were kept under standard conditions of temperature (22 ± 2 °C), light (12 h light-dark cycle) and humidity (50–70%), in individually ventilated cages, receiving standard rodent chow and tap water ad libitum. They were obtained from the Central Animal House of the Pontifícia Universidade Católica do Rio Grande do Sul (CeMBE; PUCRS; Brazil). The experimental protocol was approved by the Animal Use Ethics Committee (CEUA) of Pontifícia Universidade Católica do Rio Grande do Sul (PUCRS, CEUA 7088) and maintained in accordance with the Guiding Principles in the Care and Use of Animals approved by the Council of the American Physiological Society.

2.11. Survival curve

The animals were randomly divided in two groups and treated during the period of 15 days. The animals of the first group received intraperitoneal (i.p.) injections of CPBMF65 dissolved in olive oil (50 mg/kg daily). Mice in the second group were divided according to the dosage of CPBMF65 6, 12, 25 and 50 mg/kg (dissolved in olive oil) or vehicle (olive oil), as a negative control, and received i. p. Injections every other day (q.o.d.). After 15 days of treatment, mice were euthanized, and serological tests were performed.

2.12. Biochemical analyses

Whole blood was collected by cardiac puncture, placed in eppendorfs and centrifuged for 10 min at 2000 g. Serum aspartate aminotransferase (AST), alanine aminotransferase (ALT), total bilirubin, albumin, and alkaline phosphatase were determined with a commercial assay kit according to manufacturer's instructions (Labtest, Brazil).

2.13. Carbon tetrachloride (CCl_4)-induced liver fibrosis and treatment with CPBMF65 in mice

All drug administration was carried out at 1:00 p.m. to avoid a possible influence of circadian cycle variation on UPP1 activity. Mice received i. p. Injections of CCl_4 at the dosage of 1 ml/kg body weight (1:3 diluted in olive oil) or vehicle (olive oil) three times a week. For the treated group, animals received i. p. CCl_4 1 ml/kg (1:3 diluted in olive oil) three times a week and CPBMF65 2 mg/kg (dissolved in olive oil) twice a week. After 10 weeks of treatment, all animals were euthanized, and serum and liver sections were collected.

2.14. RNA isolation and quantitative PCR

Samples of total RNA from mouse liver tissues were extracted by Trizol reagent (Invitrogen, Thermo Fisher, Inc., USA), according to manufacturer's instructions. cDNA was synthesized from 1 μg RNA using Superscript III First-Strand Synthesis SuperMix (Invitrogen, Thermo Fisher, Inc., USA) according to the manufacturer's instructions. Primer sequences used are describe in Table 1. A final concentration of 1.4 pmol/μl for each primer and SYBR Green I Master Mix (total volume of 10 μl) were used for the reaction mix. PCR amplifications were performed in a Step One™ real-time PCR system (Applied Biosystems, Thermo Fisher, Inc., USA) using a standard protocol with annel/extend temperature of 60 °C. Reaction products were verified by melting curve analysis. All PCR reactions were performed in duplicate, and water was used as negative control. Data were analyzed with GAPDH as a reference gene. Results are expressed as fold expression relative to the expression of the control group using the ΔΔCt method.

2.15. Liver histopathology analysis

Liver samples were fixed in 10% buffered formalin, paraffin embedded, and the tissue was cut into 5 μm sections. H&E-stained liver sections (Cytological Products Soldan, Brazil) were assessed semi-quantitatively: steatosis (0–3), inflammation (0–2), and ballooning (0–2). To demonstrate fibrosis, liver sections were stained with Picrosirius Red (Polysciences, Inc., USA) Liver fibrosis also was semi-quantitatively determined: fibrosis (0–4). Images were captured through BMX 43 microscope equipped with camera DP73 (Olympus, Japan).

2.16. Statistical analysis

Results were presented using descriptive statistics (mean and standard deviation). Survival rate was analyzed by the Kaplan-Meier method (Kishore et al., 2010). For the comparison of means between groups, we have used a one-way analysis of variance (ANOVA) followed by the Tukey post-hoc test for multiple comparisons. The significance level was set at $p < 0.05$ with a 95% confidence interval. All data were analyzed using SPSS (Statistical Package for Social Sciences) version 15.0. (SPSS Inc., USA).

3. Results

3.1. Effect of CPBMF65 on GRX cell proliferation and LDH release

Firstly, we have assessed the antiproliferative effect of CPBMF65 at

Table 1
Primer sequences for RT-qPCR.

Genes	Forward primer (5′-3′)	Reverse primer (5′-3′)
GAPDH	AGTGGCAAAGTGGAGATT	GTGGAGTCATACTGGAACA
PPAR-γ	TGGAATTAGATGACAGTGACTTGG	CTCTGTGACGATCTGCCTGAG
α-SMA	ACTGGGACGACATGGAAAAG	CATCTCCAGAGTCCAGCACA
Collagen 1	GAGCGGAGAGTACTGGATCG	TACTCGAACGGGAATCCATC
Il-6	TGGAGTCACAGAAGGAGTGGCTAAG	CTGACCACAGTGAGGAATGTCCAC
TNF-α	ATAGCTCCCAGAAAAGCAAGC	CACCCCGAAGTTCAGTAGACA

doses of 7.5, 15, 45, 90 μM and NAC 400 μM (positive control) in GRX cells. Fig. 1A shows decreased proliferation at all concentrations tested. The membrane integrity of GRX cells treated with CPBMF65 was also analyzed by measuring LDH in the cell supernatant and lysate. Cells were treated with CPBMF65 (7.5 and 90 μM, the lowest and the highest concentration with significant results from our previous experiment) in order to determine its toxicity to cells. There were no significant differences between treatments and control, indicating no significant increase in cell death associated with necrosis in the treated groups as compared to the control group (Fig. 1B).

3.2. Effect of CPBMF65 on GRX cells nuclear morphology

After 120 h, we have observed an increase of nucleus phenotypically compatible with senescent cells (large and regular nuclei) in CPBMF65-treated GRX cells (7.5 and 90 μM). As expected, large and regular nuclei also increased in those cells treated with H2O2 (positive control) (Fig. 2A). We have also investigated if the decrease in cell proliferation was due to apoptosis. After 120 h, we have observed no significant difference between the CPBMF65-treated and control groups. The positive control, CDDP 2.5 μM, increased the percentage of nuclei compatibles with the apoptotic process (Fig. 2B).

3.3. Effect of CPBMF65 on GRX cell apoptosis and senescence

To confirm which mechanisms are involved in the antiproliferative effect of CPBMF65, specific analyzes for apoptosis and cell senescence were performed. The flow cytometric analysis of CPBMF65-treated cells revealed that the treatment did not reduce the number of viable cells (Fig. 3A), nor did it induce apoptosis-programmed cell death (Fig. 3B and C). Corroborating with the result found in the LDH assay (Fig. 1B), CPBMF65-treatment trigger its antiproliferative effects without causing toxicity or inducing death by necrosis (Fig. 3D). Likewise, markers for cellular senescence C_{12}FDG (Fig. 3E) and γ-H2AX (Fig. 3H) were not found in cells treated with CPBMF65, indicating that the antiproliferative effect of the compound under study is not related to the induction of death by apoptosis, nor by the induction of senescence. CDDP was used as positive control of apoptotic induction and H_2O_2 as a positive control of senescence.

3.4. CPBMF65 induces phenotypic reversion on GRX cells

The ability of CPBMF65 to revert activated HSC by inducing the accumulation of lipids in the cytoplasm was investigated. GRX cells treated with CPBMF65 showed to increase the ability of storing fat in the cytoplasm. NAC treatment also showed a significant increase in fat droplets (Fig. 4A and B). Lipid accumulation was quantified by the absorbance at 492 nm and confirmed CPBMF65 results on GRX cell storing lipids (Fig. 4B). We have also evaluated the PPAR-γ gene expression, a lipogenic intracellular factor, and found that cells treated with CPBMF65 showed a significant mRNA expression increase. We have used NAC as a control, as it is known not to increase PPAR-γ, but rather the nuclear receptor of PPAR-α.

3.5. Collagen gel contraction assay and α-SMA gene expression

After 24 h of treatment, it was possible to observe that the area occupied by the collagen gel treated with CPBMF65 or NAC was larger in comparison to the control group area. Therefore, all treatments were able to decrease cell contraction, although a greater contraction was detected in the control group, likely due to its activated phenotype (Fig. 5A). In order to verify whether GRX cells treated with CPBMF65 decreased their activation state, we also evaluated collagen and α-SMA gene expression. The α-SMA gene expression decreased significantly in the groups treated with the study compound, as well as NAC, when compared to the control group (Fig. 5B). However, collagen evaluation did not show significant changes between the studied groups (Fig. 5C).

3.6. Evaluation of CPBMF65 toxicity in vivo

Using the Kaplan-Meier survival analysis, we have evaluated the safety of CPBMF65 treatment for animals. The survival curve was

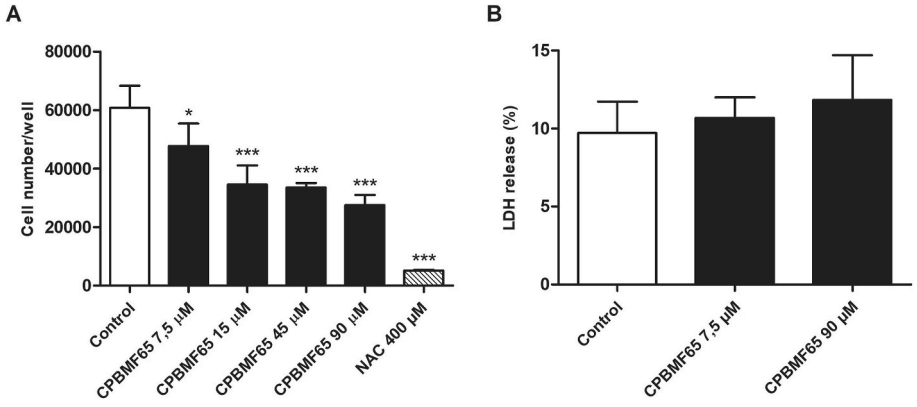

Fig. 1. Effects of CPBMF65 on GRX cells proliferation and LDH release. **(A)** GRX cells were treated with CPBMF65 (7.5–90 μM) and NAC 400 μM for 120 h and the cell number was assessed by direct cell count. Cellular proliferation was assessed by Trypan blue exclusion. Data represent the mean ± S.D. Results were expressed as cell number/well. (*P < 0.05, ***P < 0.0001 vs control, $n = 3$); **(B)** Percent of LDH release in GRX cells after 120 h of treatment with CPBMF65 7.5 and 90 μM.

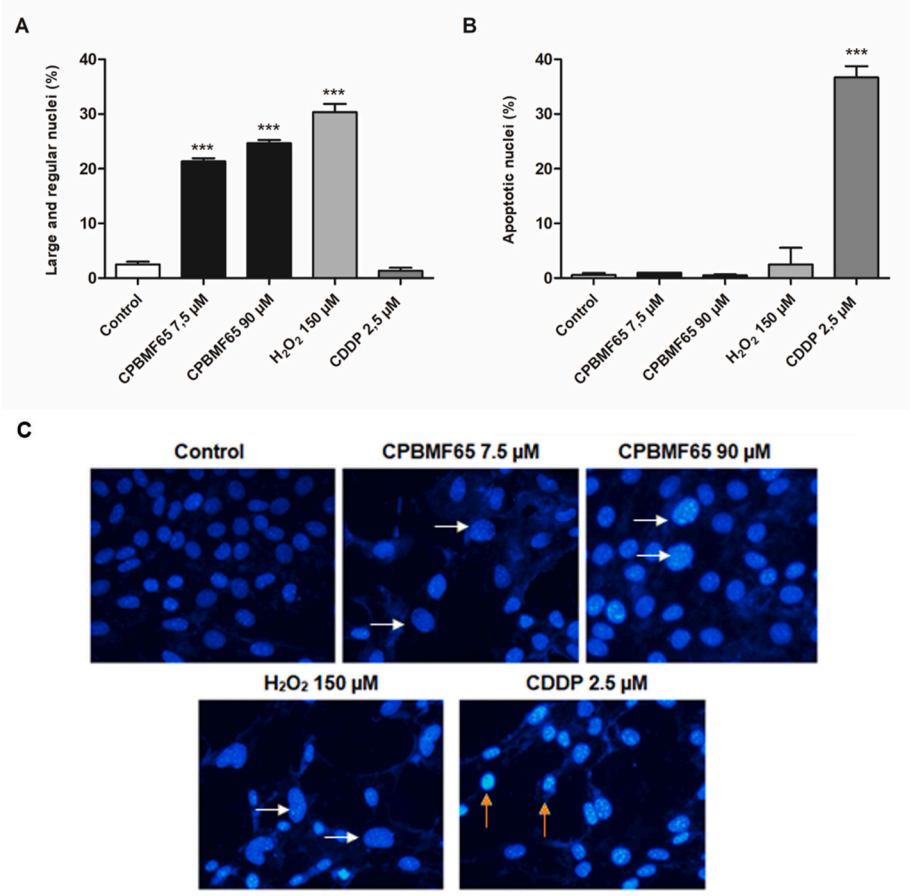

Fig. 2. DAPI nuclei staining. Effect of CPBMF65 (7.5 and 90 µM), H_2O_2 (150 µM) and CDDP (2.5 µM) on nuclear morphology of GRX cells. **(A)** Percentage of large and regular nuclei (nuclear morphology phenotypically compatible with senescent cells). **(B)** Percentage of apoptotic nuclei. **(C)** Images showing large and regular nuclei (white arrow) and apoptotic nuclei (red arrow). Cells were treated for 120 h and data presented as mean ± S.D. (***P < 0.001 vs control, n = 3). CCDP was used as positive control of apoptotic induction and H_2O_2 as a positive control of senescence.

performed using 2 treatment groups. The first group received 50 mg/kg i. p. Injections daily. After 15 days, all animals died. The second group received CPBMF65 6, 12, 25, or 50 mg/kg i. p. Injections every other day (q.o.d.). All animal survived the period of 15 days of treatment (Fig. 6A). To verify if the treatment with CPBMF65 was not toxic to the survival animals' group (CPBMF65 i. p. Injections), serological tests were performed to evaluate the levels of ALT (Fig. 6B), AST (Fig. 6C), and Total Bilirubin (Fig. 6D). The results showed that the treatment with 6–50 mg/kg q. o.d. i. p. CPBMF65 does not appear to be toxic to the liver or interfere with hepatic functions.

3.7. CCl_4 model of liver fibrosis, CPBMF65 treatment and serum analyses

Based on a previous test, we have chosen to use 2 mg/kg i. p. CPBMF65 injections, as a longer treatment period is necessary. After 10 weeks of treatment, all animals were euthanized, and serum collected and tested for hepatic parameters (Alkaline phosphatase, Albumin, AST and ALT). In the treated group (CCl_4+CPBMF65), ALT had a significant decrease in comparison to the induction group (CCl_4), showing a possible protective effect of CPBMF65 (Fig. 7D). For the other parameters, there was no significant difference between groups.

3.8. Expression of collagen I, α-SMA, IL-6 and TNF-α

The relative mRNA expression of fibrogenic genes Collagen I and α-SMA, which are related to liver fibrosis, as well as anti-inflammatory genes IL-6 and TNF-α were measured. The results show that the relative expression of Collagen I (Fig. 8A) and α-SMA (Fig. 8B) are decreased in the treated group (CCl_4+CPBMF65) when compared to the induction group (CCl_4). We have also evaluated whether CPBMF65 could decrease inflammation. Results have shown that there was a significant reduction in IL-6 (Fig. 8C), demonstrating a significant decrease in hepatic inflammation. No statistical difference was found in the TNF-α gene expression between the groups evaluated (Fig. 8D).

3.9. CPBMF65 attenuates CCl_4 induced liver injury and fibrosis

Finally, we have examined the pathological features to confirm the CPBMF65 beneficial effects. As shown in H&E staining, injection with CCl_4 induced extensive liver damage with an inflammatory cell infiltration, steatosis, and ballooning. Interestingly, the treatment with CPBMF65 decreased extensive liver damage (Fig. 9B–D). Moreover, as shown in Sirius red staining injection with CCl_4 also induced fibrotic areas in the liver tissue. Nevertheless, our results showed that CPBMF65 treatment is able to reduce this feature (Fig. 9E).

4. Discussion

Fibrosis is defined as the overgrowth, hardening, or scarring of tissues that could be transformed in a major tissue damage, contributing to a variety of diseases, such as cirrhosis. There is no standard treatment for liver fibrosis, but several studies have revealed targets to prevent fibrosis progression (Bataller and Brenner, 2005; Povero et al., 2010). In this study, we evaluated the effect of CPBMF65, a synthetic UPP1 inhibitory molecule, as a possible molecule with therapeutic use to liver fibrosis. The UPP1 enzyme catalyzes the reversible phosphorolytic cleavage of uridine. CPBMF65 is an inhibitor of UPP1, leading to a potential increase of intracellular Urd. The Urd inhibits inflammation and fibrosis in a bleomycin-induced model of lung injury, decreasing collagen production (Cicko et al., 2015). Although Urd can have a protective effect, it is known that exogenous administration of Urd is not well tolerated, since higher doses would have to be administered in order to obtain

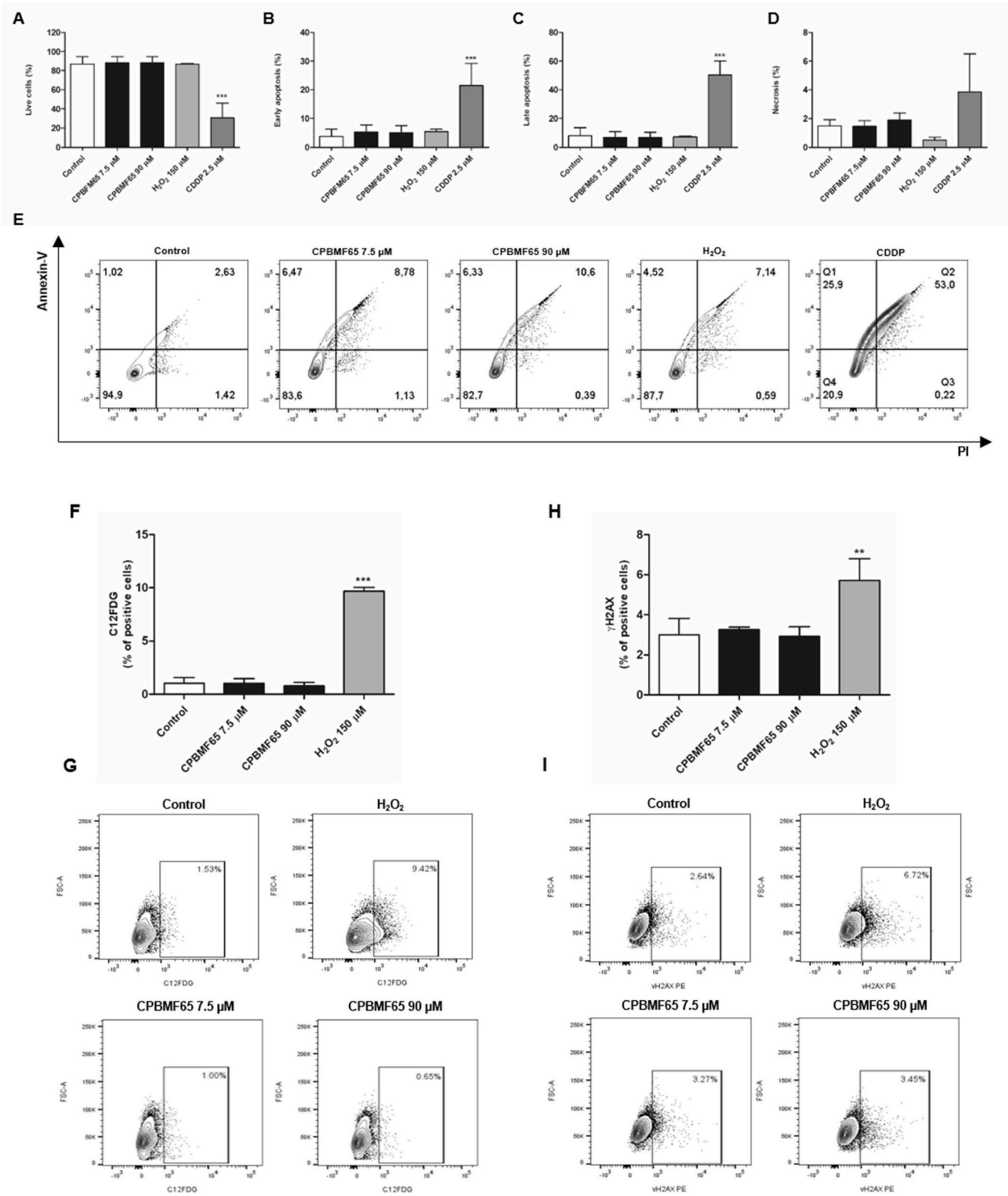

Fig. 3. Antiproliferative mechanisms of CPBMF65. Results of apoptosis induction are expressed as percentage of **(A)** live cells, **(B)** early apoptosis, **(C)** late apoptosis and **(D)** necrosis. **(E)** Representative flow cytometric plots of control and treatments group (CPBMF65, H_2O_2, and CDDP). Results of markers for cellular senescence are expressed as percentage of **(F)** C_{12}FDG and **(H)** γ-H2AX. **(G–I)** Representative flow cytometric plots of control and treatments group (CPBMF65 and H_2O_2). Cells were treated for 120 h and data presented as mean ± S.D. (***$P < 0.001$ vs control, $n = 3$). CDDP was used as positive control of apoptotic induction and H_2O_2 as a positive control of senescence.

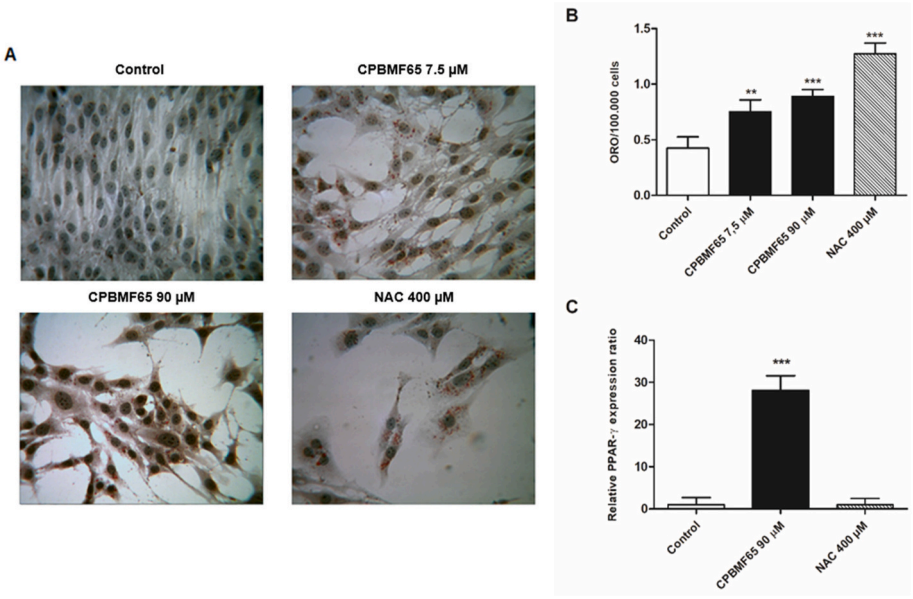

Fig. 4. Phenotypic reversion on GRX cells. **(A)** Oil Red-O (ORO) staining of GRX cells at 120 h for control, CPBMF65 7.5 and 90 µM, and NAC 400 µM; **(B)** Lipid quantification of GRX cells; **(C)** Relative mRNA expression ratio of PPAR-γ. Results are shown as the absorbance value obtained for ORO adjusted for 5×10^4 cells. Data presented as mean ± S.D. (**P < 0.01, ***P < 0.001 vs control, n = 3).

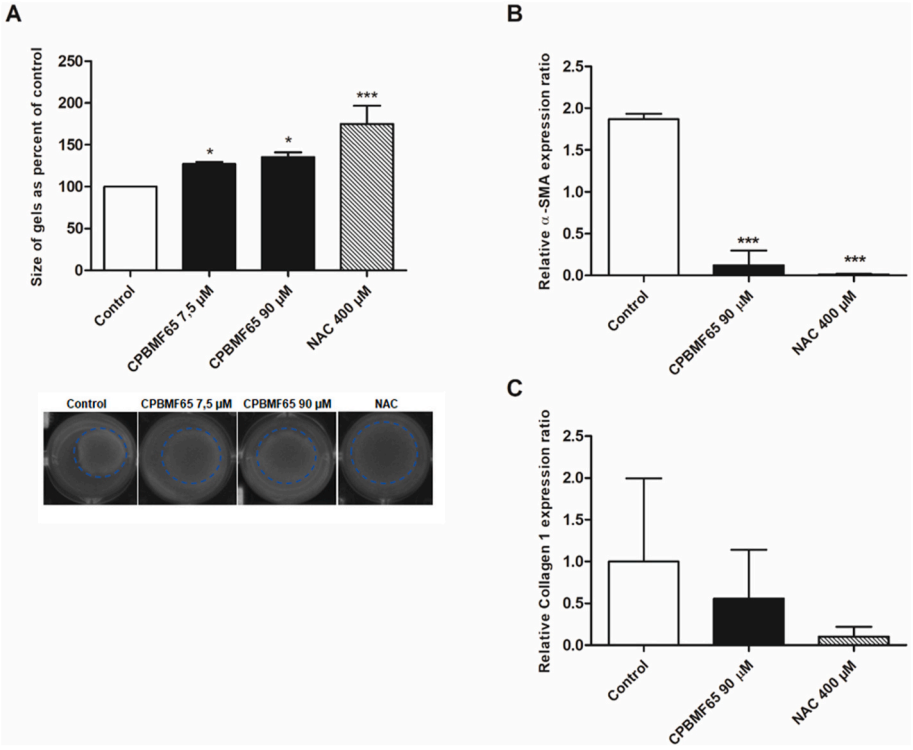

Fig. 5. Contractile profile of GRX cells treated with CPBMF65 **(A)** Cell contraction assessed by collagen gel assay in GRX cells. **(B)** Relative mRNA expression ratio of α-SMA. **(C)** Relative mRNA expression ratio of collagen 1. Cells were treated for 24 h and data presented as mean ± S.D. (*P < 0.05, ***P < 0.001 vs control, n = 3).

significant effects, due to the rapid degradation caused by UPP1. Thus, molecules target which inhibition of UPP1 enzyme, as CPBMF65, has great therapeutic potential.

Once intracellular Urd increases, it is possible to reduce cell proliferation, as this increase reflects the partial halt of the salvage pathway. The salvage pathway operates to recover bases and nucleosides generated from the breakdown of DNA and RNA. The salvaged bases can be then transformed into nucleotides and reincorporated into DNA. Nucleotides and nucleosides are regenerated contributing to DNA formation, thus reactivating cell proliferation and growth (Squadrito et al., 2017). Previous studies showed an association between pyrimidine metabolism and liver diseases, suggesting that Urd may have a protective effect in chronic liver diseases (Schofield et al., 2017). In hepatocarcinoma HepG2 cells, treatment with CPBMF65 increased the intracellular uridine levels and reduced cancer cell proliferation through cell cycle arrest, without causing toxicity (da Silva et al., 2020).

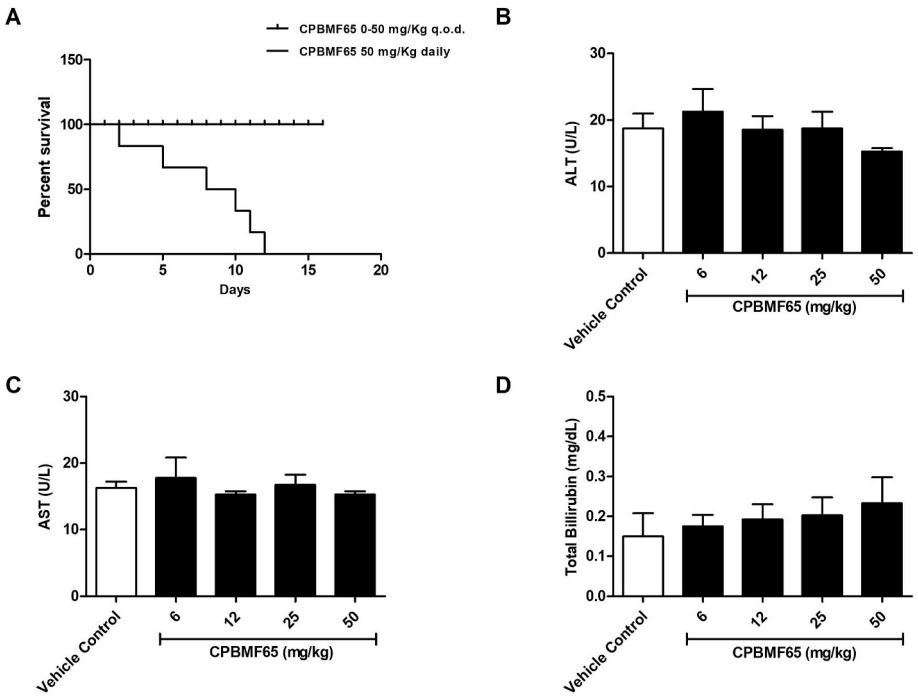

Fig. 6. CPBMF65 toxicity *in vivo*. **(A)** Kaplan-Meier survival curve analyses during the treatment period. The curve is different between daily and q. o.d. Groups (***P < 0.001). P- value was calculated by the log-Rank test. Hepatic parameters evaluated were **(B)** ALT (U/L), **(C)** AST (U/L) and **(D)** Total Bilirubin (mg/dl). Data presented as mean ± S.D. No significant differences were found.

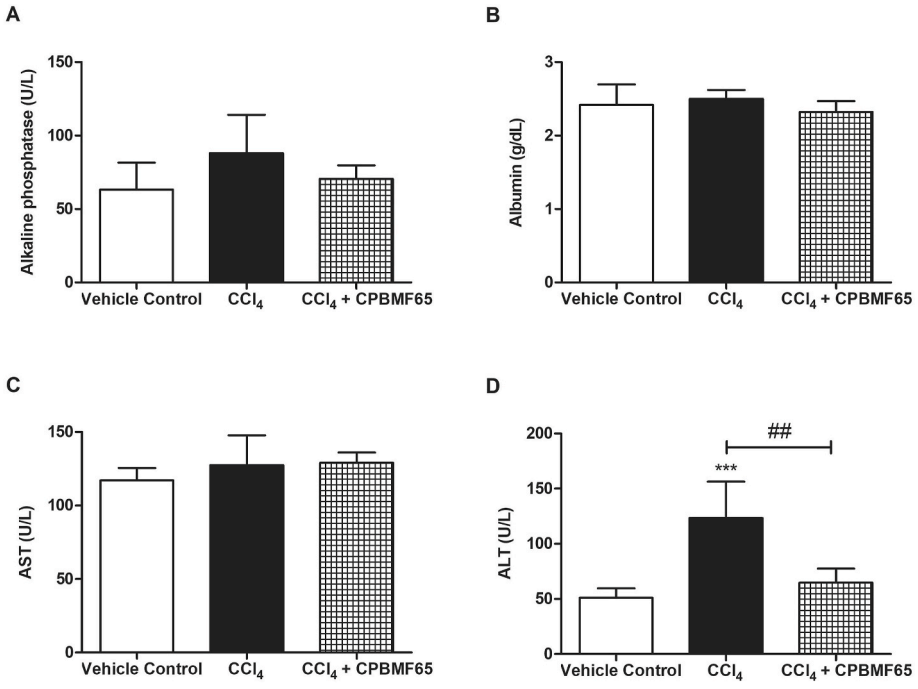

Fig. 7. Serum analyses of hepatic parameters: **(A)** Alkaline phosphatase (U/L), **(B)** Albumin (g/dl), **(C)** AST (U/L), and **(D)** ALT (U/L). Data presented as mean ± S.D. (***P < 0.001 vs control, ##P < 0.05 CCl_4 vs CCl_4+CPBMF65).

Our findings have shown a reduced proliferation at doses 7.5–90 μM in GRX cells when compared to control (cells that received no treatment). NAC was used as a positive control. Reduction of proliferation in GRX cells is usually caused by necrosis (cytotoxicity) or cell programed death mechanisms. Therefore, aiming to demonstrate that this effect was not due to cytotoxicity, LDH was measured and there was no correlation between the ceasing of cell proliferation and death due to necrosis in GRX cells. We have also used trypan blue, which demonstrated absence of necrosis as well. Inhibition of cell proliferation and induction of apoptosis are recognized as potent antiproliferative mechanisms to block the activation of HSCs. Also, the induction of senescence is an additional mechanism that may be involved in the reversion of activated HSC preventing and treating liver fibrosis (Krizhanovsky et al., 2008). Through the nuclear morphometric analysis, we verified that the cells

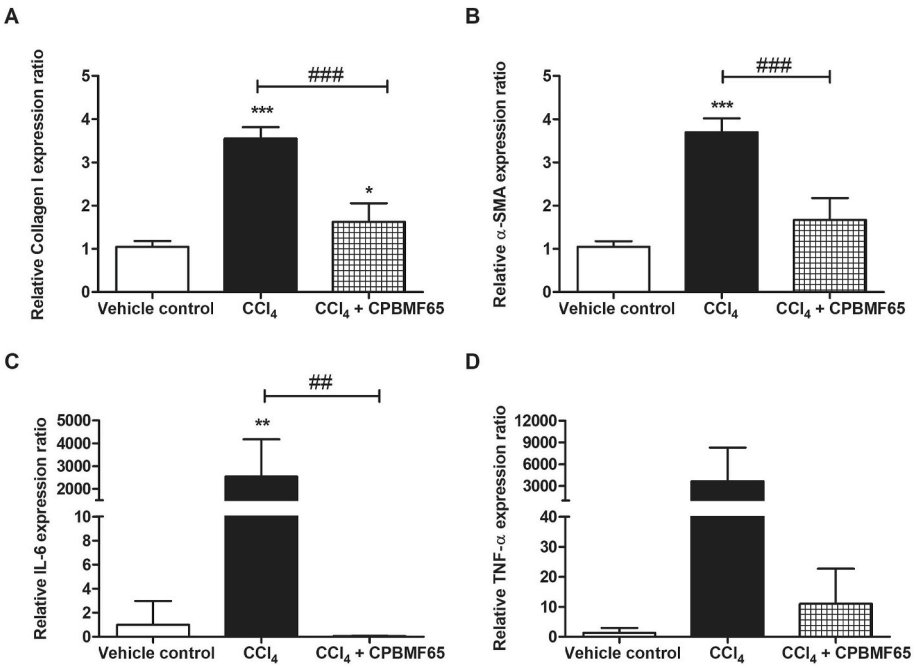

Fig. 8. Effect of CCl_4 induction and CPBMF65 treatment on the relative mRNA expression ratio of **(A)** Collagen I, **(B)** α-SMA, **(C)** IL-6 and **(D)** TNF-α in mouse liver tissue. Data presented as mean ± S.D. (*P < 0.05 and ***P < 0.001 vs control, ###P < 0.001 CCl_4 vs CCl_4+CPBMF65).

submitted to treatment with CPBMF65 did not present nuclear morphology compatible with apoptotic cells. This data was confirmed through the evaluation of apoptosis by flow cytometry, demonstrating that the antiproliferative effect of CPBMF65 in GRX cells was not due to programmed cell death due to apoptosis. Even that nuclear cellular morphology shows an increase in nucleus phenotypically compatible with senescent cells (large and regular nuclei), we demonstrated by two different markers (C_{12}FDG and γ-H2AX) that CPBMF65 does not induces an irreversible cell cycle arrest by senescence.

GRX cells are an immortalized lineage of hepatic stellate liver cells that present the myofibroblast transitional phenotype, being between the quiescent and activated states (Herrmann et al., 2007). HSCs serve as the main body storage compartment for vitamin A through lipid droplets. In the presence of liver injury and profibrogenic cytokines, HSCs acquire an activated phenotype, characterized by an elevated expression of extracellular matrix, greater ability to contract, production of collagen I and α-SMA fibers, associated to lipid droplets loss (Bobowski-Gerard et al., 2018). On the other hand, some molecules, such as retinol, retinoic acid, or drugs that modify lipid metabolism such as indomethacin (anti-inflammatory) are able to revert the activated phenotype to quiescent. The quiescent phenotype can be achieved by the reorganization of actin cytoskeleton and accumulation of fat droplets in the cytoplasm. (Guimaraes et al., 2006). In its quiescent state, besides presenting lipid inclusions (droplets) containing retinol, HSCs have a round and large nucleus (Passino et al., 2007). The increase in nucleus size found in treated cells occurs because the CPBMF65 treatment modulates the activated phenotype of HSCs (GRX) to the quiescent phenotype.

When in an activated phenotype (myofibroblast-like), HSC cells can proliferate and synthase profibrotic factors. On the other hand, in the quiescent phenotype the GRX cells have a decrease of profibrotic factors release. Our study revealed a significant increase of lipid droplets, evidenced by ORO staining, meaning that there was a deactivation of the GRX cells. To better understand this phenotypic reversal, we have evaluated gene expression of collagen and α-SMA, important molecules involved in the transformation of quiescent stellate cells into the myofibroblastic phenotype, and found a significant decrease in α-SMA mRNA levels in cells treated with CPBMF65. We have also evaluated the expression of PPAR-γ, an important factor in the lipid synthesis pathway, and observed a significant increase with treatment, as well as a reduction of contraction assessed by the collagen gel assay.

In the first moment, we revealed the therapeutic effect of CPBMF65 in a lineage of GRX cells. However, to investigate the *in vivo* relevance of our findings, we also investigate the effect of CPBMF65 treatment in a mouse model of liver fibrosis. The i. p. Treatment with CPBMF65, on alternate days, in BALB/c males proved to be safe for the animals, as indicated by both the survival curve and the serological testes for liver parameters. In an attempt to prevent the liver damage induced by CCl_4 in mice, CPBMF65 2 mg/kg i. p. Injections were used over the period of induction. The *in vivo* experiments demonstrated that CCl_4 treatment did not induce cholestasis, as assessed by serological measurement of alkaline phosphatase, nor did it decrease its function, since serum albumin concentrations did not change in any of the groups studied. We also did not observe changes in AST serological levels, a marker of cell necrosis, but a significant increase in ALT enzyme was seen, which means that CCl_4 damaged the liver, but did not cause necrosis, only increased the cell membrane permeability. Similar results were found in the study of D'Argenio et al., (2010) (D'Argenio et al., 2010). In our liver fibrosis model, the levels of ALT are elevated, as a result of increased hepatic injury caused by the CCl_4 induction. Interestingly, the animals that received CPBMF65 treatment have a decrease in levels of ALT, suggesting a protective effect.

The inflammation plays a central role in tissue damage and is closely related to hepatic fibrosis development. This inflammation is mediated by proinflammatory cytokines, such as TNF-α and IL-6 (Koyama and Brenner, 2017). Thus, we also explored the ability of CPBMF65 to decrease inflammation. Although treatment with CPBMF65 demonstrates a tendency to decrease TNF-α mRNA expression, we did not find any significant difference after this treatment time. Nevertheless, the IL-6 mRNA expression was reduced in animals treated with CPBMF65. Since CPBMF65 was capable that attenuates the IL-6 mRNA expression we also investigated its effects over profibrotic markers. Was observed that the treatment with CPBMF65 reduced the mRNA expression of collagen I and α-SMA. Furthermore, corroborating with our results, the histopathologic analysis shows that animals that were submitted to the model of liver fibrosis by CCl_4 injection feature an increase of steatosis,

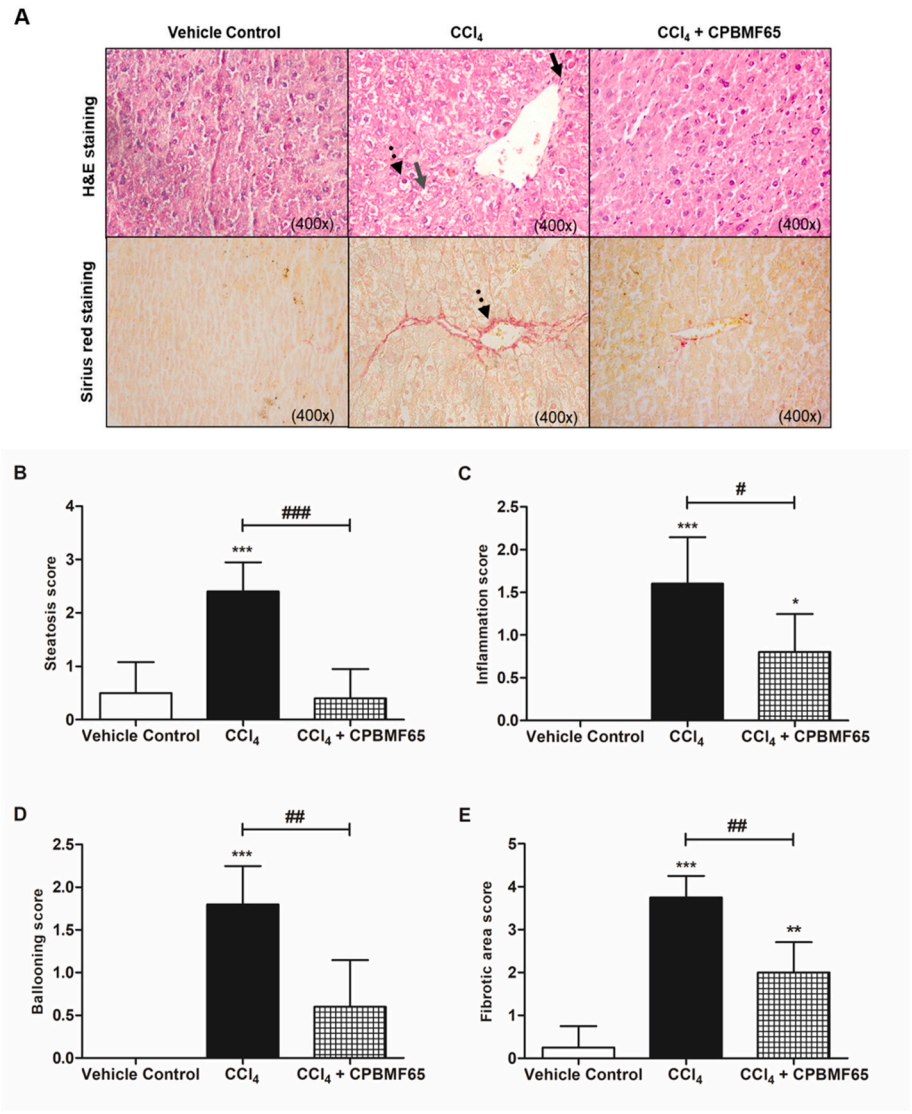

Fig. 9. CPBMF65 administration reduces CCl_4-induced liver fibrosis in mice. **(A)** Images of H&E staining (top) and Sirius red staining (bottom). Dotted black arrow indicates steatosis (H&E staining) and a fibrotic area (Sirius red staining); grey arrow indicates ballooning; black arrow indicates inflammation. **(B)** Steatosis score, **(C)** Inflammation score, **(D)** Ballooning score, and **(E)** Fibrotic area score. Data presented as mean ± S.D. (*P < 0.05, **P < 0.01 and. ***P < 0.001 vs control, #P < 0.05, ##P < 0.01 and ###P < 0.001 CCl_4 vs CCl_4+CPBMF65).

inflammation, ballooning, and fibrotic area. Meanwhile, the animals that were treated with CPBMF65 reduces these parameters.

In summary, our data reveal that CPBMF65 does not induces cellular death by apoptosis, or by senescence in activated hepatic stellates cells (GRX cell line). The CPBMF65 treatment was able to induce phenotypic reversion in GRX cells through the ability to induce the store fat in the cell cytoplasm. In a model of liver fibrosis in mice, our findings showed that treatment with CPBMF65 was capable to decrease pro-inflammatory and profibrotic markers, improving the pathological features in liver tissue. Taken together, our results revealed, for the first time, that CPBMF65 should be considered in future studies as a potential agent to treat liver fibrosis.

CRediT authorship contribution statement

Elisa Feller Gonçalves da Silva: Conceptualization, Data curation, Formal analysis, Writing - original draft. **Bruna Pasqualotto Costa:** Data curation, Formal analysis, Writing - review & editing. **Marcella Tornquist Nassr:** Data curation, Validation. **Bruno de Souza Basso:** Data curation, Formal analysis, Writing - review & editing. **Matheus Scherer Bastos:** Data curation, Formal analysis, Validation. **Géssica Luana Antunes:** Data curation, Formal analysis, Writing - review & editing. **Camille Kirinus Reghelin:** Data curation, Validation. **Maria Claudia Rosa Garcia:** Data curation, Validation. **Vitor Giancarlo Schneider Levorse:** Data curation, Validation. **Leonardo Pfeiff Carlessi:** Data curation, Validation. **Krist Helen Antunes Fernandes:** Data curation, Validation. **Carine Raquel Richter Schmitz:** Data curation, Validation. **Gabriela Viegas Haute:** Data curation, Validation. **Carolina Luft:** Data curation, Validation. **Eliane Santarém:** Formal analysis, Project administration. **Florencia María Barbé-Tuana:** Formal analysis, Project administration. **Márcio Vinícius Fagundes Donadio:** Formal analysis, Project administration. **Luiz Augusto Basso:** Formal analysis, Project administration. **Pablo Machado:** Conceptualization, Formal analysis, Project administration, Writing - original draft. **Jarbas Rodrigues de Oliveira:** Conceptualization, Formal analysis, Project administration, Writing - original draft.

Declaration of competing interest

The authors declare no conflict of interest.

Acknowledgements

This study was financed, in part, by the Coordenação de Aperfeiçoamento de Pessoal de Nível Superior (CAPES), Brasil. Finance Code 001.

References

Bárcena, C., Aran, G., Perea, L., Sanjurjo, L., Téllez, É., Oncins, A., Masnou, H., Serra, I., García-Gallo, M., Kremer, L., Sala, M., Armengol, C., Sancho-Bru, P., Sarrias, M.-R., 2019. CD5L is a pleiotropic player in liver fibrosis controlling damage, fibrosis and immune cell content. EBioMedicine 43, 513–524. https://doi.org/10.1016/j.ebiom.2019.04.052.

Basso, B. de S., de Mesquita, F.C., Dias, H.B., Krause, G.C., Scherer, M., Santarém, E.R., de Oliveira, J.R., 2019. Therapeutic effect of baccharis anomala dc. Extracts on activated hepatic stellate cells. EXCLI J. https://doi.org/10.17179/excli2018-1696.

Bataller, R., Brenner, D.A., 2005. Liver fibrosis. J. Clin. Invest. 115, 209–218. https://doi.org/10.1172/JCI24282.

Bobowski-Gerard, M., Zummo, F., Staels, B., Lefebvre, P., Eeckhoute, J., 2018. Retinoids issued from hepatic stellate cell lipid droplet loss as potential signaling molecules orchestrating a multicellular liver injury response. Cells 7, 137. https://doi.org/10.3390/cells7090137.

Cicko, S., Grimm, M., Ayata, K., Beckert, J., Meyer, A., Hossfeld, M., Zissel, G., Idzko, M., Müller, T., 2015. Uridine supplementation exerts anti-inflammatory and anti-fibrotic effects in an animal model of pulmonary fibrosis. Respir. Res. 16, 105. https://doi.org/10.1186/s12931-015-0264-9.

D'Argenio, G., Amoruso, D.C., Mazzone, G., Vitaglione, P., Romano, A., Ribecco, M.T., D'Armiento, M.R., Mezza, E., Morisco, F., Fogliano, V., Caporaso, N., 2010. Garlic extract prevents CCl4-induced liver fibrosis in rats: the role of tissue transglutaminase. Dig. Liver Dis. 42, 571–577. https://doi.org/10.1016/j.dld.2009.11.002.

da Silva, E.F.G., Lima, K.G., Krause, G.C., Haute, G.V., Pedrazza, L., Catarina, A.V., Gassen, R.B., de Souza Basso, B., Dias, H.B., Luft, C., Garcia, M.C.R., Costa, B.P., Antunes, G.L., Basso, L.A., Donadio, M.V.F., Machado, P., de Oliveira, J.R., 2020. CPBMF65, a synthetic human uridine phosphorylase-1 inhibitor, reduces HepG2 cell proliferation through cell cycle arrest and senescence. Invest. N. Drugs. https://doi.org/10.1007/s10637-020-00941-2.

De Mesquita, F.C., Bitencourt, S., Caberlon, E., Da Silva, G.V., Basso, B.S., Schmid, J., Ferreira, G.A., De Oliveira, F.D.S., De Oliveira, J.R., 2013. Fructose-1,6-bisphosphate induces phenotypic reversion of activated hepatic stellate cell. Eur. J. Pharmacol. 720, 320–325. https://doi.org/10.1016/j.ejphar.2013.09.067.

Debacq-Chainiaux, F., Erusalimsky, J.D., Campisi, J., Toussaint, O., 2009. Protocols to detect senescence-associated beta-galactosidase (SA-βgal) activity, a biomarker of senescent cells in culture and in vivo. Nat. Protoc. 4, 1798–1806. https://doi.org/10.1038/nprot.2009.191.

Guimaraes, E.L.M., Franceschi, M.F.S., Grivicich, I., Dal-pizzol, F., Moreira, J.C.F., Guaragna, R.M., Borojevic, R., Margis, R., Guma, F.C.R., 2006. Relationship between oxidative stress levels and activation state on a hepatic stellate cell line. Liver Int. 26, 477–485. https://doi.org/10.1111/j.1478-3231.2006.01245.x.

Herrmann, J., Gressner, A.M., Weiskirchen, R., 2007. Immortal hepatic stellate cell lines: useful tools to study hepatic stellate cell biology and function? J. Cell Mol. Med. 11, 704–722. https://doi.org/10.1111/j.1582-4934.2007.00060.x.

Kim, T.M., Shin, S.K., Kim, T.W., Youm, S.Y., Kim, D.J., Ahn, B., 2012. Elm tree bark extract inhibits HepG2 hepatic cancer cell growth via pro-apoptotic activity. J. Vet. Sci. https://doi.org/10.4142/jvs.2012.13.1.7.

Kishore, J., Goel, M., Khanna, P., 2010. Understanding survival analysis: Kaplan-Meier estimate. Int. J. Ayurveda Res. 1, 274. https://doi.org/10.4103/0974-7788.76794.

Koyama, Y., Brenner, D.A., 2017. Liver inflammation and fibrosis. J. Clin. Invest. 127, 55–64. https://doi.org/10.1172/JCI88881.

Krizhanovsky, V., Yon, M., Dickins, R.A., Hearn, S., Simon, J., Miething, C., Yee, H., Zender, L., Lowe, S.W., 2008. Senescence of activated stellate cells limits liver fibrosis. Cell 134, 657–667. https://doi.org/10.1016/j.cell.2008.06.049.

Passino, M.A., Adams, R.A., Sikorski, S.L., Akassoglou, K., 2007. Regulation of hepatic stellate cell differentiation by the neurotrophin receptor p75NTR. Science 315, 1853–1856. https://doi.org/10.1126/science.1137603 (80).

Pizzorno, G., Cao, D., Leffert, J.J., Russell, R.L., Zhang, D., Handschumacher, R.E., 2002. Homeostatic control of uridine and the role of uridine phosphorylase: a biological and clinical update. Biochim. Biophys. Acta (BBA) - Mol. Basis Dis. 1587, 133–144. https://doi.org/10.1016/S0925-4439(02)00076-5.

Povero, D., Busletta, C., Novo, E., Di Bonzo, L.V., Cannito, S., Paternostro, C., Parola, M., 2010. Liver fibrosis: a dynamic and potentially reversible process. Histol. Histopathol. https://doi.org/10.14670/HH-25.1075.

Rajan, N., Habermehl, J., Coté, M.-F., Doillon, C.J., Mantovani, D., 2006. Preparation of ready-to-use, storable and reconstituted type I collagen from rat tail tendon for tissue engineering applications. Nat. Protoc. 1, 2753–2758. https://doi.org/10.1038/nprot.2006.430.

Renck, D., Ducati, R.G., Palma, M.S., Santos, D.S., Basso, L.A., 2010. The kinetic mechanism of human uridine phosphorylase 1: towards the development of enzyme inhibitors for cancer chemotherapy. Arch. Biochem. Biophys. 497, 35–42. https://doi.org/10.1016/j.abb.2010.03.004.

Renck, D., MacHado, P., Souto, A.A., Rosado, L.A., Erig, T., Campos, M.M., Farias, C.B., Roesler, R., Timmers, L.F.S.M., De Souza, O.N., Santos, D.S., Basso, L.A., 2013. Design of novel potent inhibitors of human uridine phosphorylase-1: synthesis, inhibition studies, thermodynamics, and in vitro influence on 5-fluorouracil cytotoxicity. J. Med. Chem. https://doi.org/10.1021/jm401389u.

Schofield, Z., Reed, M.A.C., Newsome, P.N., Adams, D.H., Günther, U.L., Lalor, P.F., 2017. Changes in human hepatic metabolism in steatosis and cirrhosis. World J. Gastroenterol. 23, 2685. https://doi.org/10.3748/wjg.v23.i15.2685.

Sharma, A., Singh, K., Almasan, A., 2012. Histone H2AX phosphorylation: a marker for DNA damage, pp. 613–626. https://doi.org/10.1007/978-1-61779-998-3_40.

Shin, G.-M., Koppula, S., Chae, Y.-J., Kim, H.-S., Lee, J.-D., Kim, M.-K., Song, M., 2018. Anti-hepatofibrosis effect of Allium senescens in activated hepatic stellate cells and thioacetamide-induced fibrosis rat model. Pharm. Biol. 56, 632–642. https://doi.org/10.1080/13880209.2018.1529801.

Sperotto, R.A., 2014. Protocolos e métodos de análise em laboratórios de biotecnologia agroalimentar e de saúde humana. Editora Univates. https://doi.org/10.13140/RG.2.1.4693.0645.

Squadrito, F., Bitto, A., Irrera, N., Pizzino, G., Pallio, G., Minutoli, L., Altavilla, D., 2017. Pharmacological activity and clinical use of PDRN. Front. Pharmacol. 8 https://doi.org/10.3389/fphar.2017.00224.

Weinberg, M.E., Roman, M.C., Jacob, P., Wen, M., Cheung, P., Walker, U.A., Mulligan, K., Schambelan, M., 2011. Enhanced uridine bioavailability following administration of a triacetyluridine-rich nutritional supplement. PloS One 6, e14709. https://doi.org/10.1371/journal.pone.0014709.

Zdanov, S., 2006. Establishment of H2O2-induced premature senescence in human fibroblasts concomitant with increased cellular production of H2O2. Ann. N. Y. Acad. Sci. 1067, 210–216. https://doi.org/10.1196/annals.1354.025.